Computational Electromagnetics: Current Applications and Future Trends

D. Govan, E. Bekker, J. D. Paul, S. Greedy, Y. Liu, K. Biwojno, J. Wykes, A. Vukovic, D. W. P. Thomas, T. M. Benson, P. Sewell and C. Christopoulos

Abstract – **This paper examines the numerical techniques used to model aspects of EMC and photonics design. A short review of popular numerical techniques will be given and recent developments in several areas will be examined, including the description of fine wires, complex material properties, optical modulators and the use of unstructured meshes.**

Keywords – **Computational Electromagnetics, Time-domain simulation**

I. INTRODUCTION

The modelling of electromagnetic problems can be of great benefit over a wide range of applications. Two areas in particular where the use of numerical techniques at the design stage can lead to time and cost savings are Electromagnetic Compatibility (EMC) and the development of photonic components. In these areas, time domain modelling techniques such as Transmission Line Modelling (TLM) [1] and Finite Difference Time Domain modelling (FDTD) [2] have proved to be flexible and powerful tools. Finite Element modelling [3] and the Method of Moments [4] are also frequently used techniques. In photonics modelling it is often sufficient to model the slowly varying envelope without explicitly modelling the rapidly varying aspects of the electromagnetic field. The Finite Difference Beam Propagation Method (FD-BPM) [5] is the most widely used method in this area. For some configurations, when certain approximations are valid, other techniques such as the Spectral Index (SI) [6] method or the Free Space Radiation Mode Method (FSRM) [7] can be used to improve the speed of the calculation. More recently Integral Equations Formulations in both frequency [8] and time [9] domains have proved highly effective when applied to the simulation of a wide range of photonics structures.

Despite the rapid increase in computer performance over the years there are several areas of electromagnetic simulation that cannot be fully investigated. Multi-scale problems in EMC such as fine wires in equipment cabinets, thin panels, fine conducting tracks and other small features cannot be efficiently modelled without making modifications to the standard techniques. The fine grid required to describe all the fine features in a relatively large problem would need an impractically large amount of memory and processor time to be of use. Both TLM and FDTD allow the use of more efficient techniques such as finding a local solution for the field around the fine feature and mapping this onto the global problem or distorting the numerical grid around the fine feature to give an accurate description of this feature without having to finely grid the rest of the problem. These techniques will be described more fully in this paper.

One recent advance that has improved the modelling of fine features is the use of unstructured triangular meshes in TLM rather than rectangular meshes [10]. Triangular meshes can improve models in several areas. Some examples are as an interface between fine and course meshes in a multi-scale problem and to give a better description of areas of a problem that are not rectangular in shape [11]. More details of these will also be given in this paper.

Another aspect of TLM that will be described here is its use to investigate the response of materials. Time domain techniques such as TLM and FDTD are of particular use when describing the interaction of electromagnetic waves and materials because a single simulation can be used to study the material response over a wide bandwidth. Using frequency domain techniques several simulations would be required to cover the same bandwidth. TLM is particularly well suited to studying materials with frequency dependent or nonlinear properties as well as anisotropic materials. Some of the work done in this area will be described in section III (C).

Several areas of Electromagnetic modelling involve the description of more than one signal type. An example of this is an optical modulator. In these devices a microwave signal is used to modulate an optical signal. The design of these devices requires the accurate modelling of both the microwave and optical responses of the device to optimise the design. Section III (D) describes the use of the TLM method in the design of an electroabsorption modulator.

Finally a description of the use of FD-BPM to model and optimise photonics components such as tapered laser cavities will be given.

This paper contains a review of some of the numerical techniques developed and used by members of the George Green Institute for Electromagnetics Research, University of Nottingham. These include TLM, and FD-BPM. There follows specific examples of practical areas where these techniques have been used and conclusions.

II. NUMERICAL TECHNIQUES

This section will give a brief description of some of the numerical techniques used in computational electromagnetics, including Transmission Line Method (TLM), and the Finite Difference Beam Propagation Method (FD-BPM).

Authors are from the George Green Institute for Electromagnetics Research, University of Nottingham, Nottingham NG7 2RD, UK Email: donald.govan@nottingham.ac.uk

A. Transmission Line Modelling

TLM is a method of solving Maxwell's equations, which may be expressed as

$$\begin{bmatrix} \nabla \times \underline{H} \\ -\nabla \times \underline{E} \end{bmatrix} = \begin{bmatrix} \underline{J}_e \\ \underline{J}_m \end{bmatrix} + \frac{\partial}{\partial t} \begin{bmatrix} \underline{D} \\ \underline{B} \end{bmatrix} \tag{1}$$

The constitutive relations for the current and voltage densities for isotropic media are given by,

$$\begin{bmatrix} \underline{J}_e \\ \underline{J}_m \end{bmatrix} = \begin{bmatrix} \underline{J}_{ef} + \sigma_e * \underline{E} \\ \underline{J}_{mf} + \sigma_m * \underline{H} \end{bmatrix} \tag{2}$$

where * indicates a time-domain convolution. The constitutive relations for the flux densities are given by,

$$\begin{bmatrix} \underline{D} \\ \underline{B} \end{bmatrix} = \begin{bmatrix} \varepsilon_0 \underline{E} + \varepsilon_0 \chi_e * \underline{E} \\ \mu_0 \underline{H} + \mu_0 \chi_m * \underline{H} \end{bmatrix} \tag{3}$$

substituting (2) and (3) in (1) gives,

$$\begin{bmatrix} \nabla \times \underline{H} \\ -\nabla \times \underline{E} \end{bmatrix} - \begin{bmatrix} J_{ef} \\ J_{mf} \end{bmatrix} = \begin{bmatrix} \sigma_e * \underline{E} \\ \sigma_m * \underline{H} \end{bmatrix} + \frac{\partial}{\partial t} \begin{bmatrix} \varepsilon_0 \underline{E} + \varepsilon_0 \chi_e * \underline{E} \\ \mu_0 \underline{H} + \mu_0 \chi_m * \underline{H} \end{bmatrix} \tag{4}$$

The electric and magnetic fields along with the current and voltage densities are then normalised to have the dimension volts. A TLM cell with dimensions $\Delta z = \Delta y = \Delta z = \Delta l$ is chosen as shown in Fig 1. Although this cell does not have to be cubical, a cubic node is considered here for simplicity. Following normalisation the electric and magnetic fields become

$$\underline{E} = -\underline{V} \Big/ \Delta l \qquad \underline{H} = -\underline{i} \Big/ \Delta l \eta_0 \tag{5}$$

where Δl is a space step and η_0 is the intrinsic impedance of free space. Similarly the electric and magnetic free-current densities are also normalised to quantities with the dimension volts

$$\underline{J}_{ef} = -\underline{i}_f \Big/ \left(\Delta l^2 \eta_0\right), \qquad \underline{J}_{mf} = -\underline{V}_f \Big/ \Delta l^2 \tag{6}$$

the time and space derivatives are also normalised.

$$\frac{\partial}{\partial t} = \frac{1}{\Delta \bar{t}} \frac{\partial}{\partial \bar{t}}, \qquad \left(\nabla \times ...\right) = \frac{1}{\Delta l} \left(\bar{\nabla} \times ...\right) \tag{7}$$

Where the maximum time step for the TLM algorithm is given by [1]

$$\Delta t = \frac{\Delta l}{2c} \tag{8}$$

where c is the speed of light in vacuum. The free-space permittivity and permeability are included in the model through the transmission line capacitance and inductance respectively

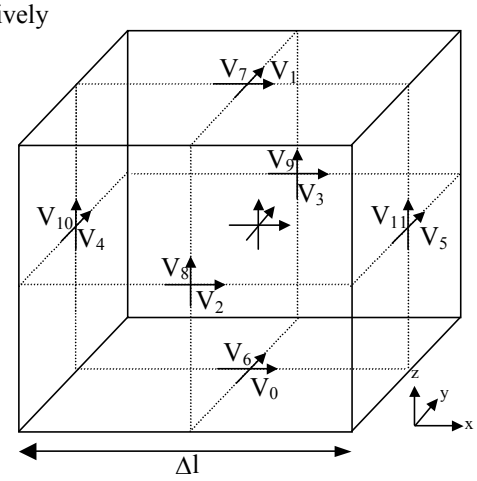

Fig. 1. 3-D TLM Cell

After these normalisations Maxwell's equations in free space become

$$\begin{bmatrix} \bar{\nabla} \times \underline{i} \\ -\bar{\nabla} \times \underline{V} \end{bmatrix} - \begin{bmatrix} \underline{i}_f \\ \underline{V}_f \end{bmatrix} - 2 \frac{\partial}{\partial \bar{t}} \begin{bmatrix} \underline{V} \\ \underline{i} \end{bmatrix} = 0 \tag{9}$$

This equation is mapped onto the cell shown in Fig 1. The curl equations can then be calculated using Stoke's theorem. For example

$$\left(\bar{\nabla} \times \underline{V}\right)_z = -\left(V_2 - V_3 - V_4 + V_5\right) \tag{10}$$

The total voltages can be obtained from the incident voltages to the cell, i.e. $V_4 = 2V_4^i - i_z$ where,

$$i_z = -\frac{1}{2}\left(V_2^i - V_3^i - V_4^i + V_5^i\right) - \frac{1}{4} V_{fz} \tag{11}$$

where i indicates an incident voltage.

Equation (9) can now be expressed as,

$$\begin{bmatrix} V_x \\ V_y \\ V_z \\ i_x \\ i_y \\ i_z \end{bmatrix} = \frac{1}{2} \begin{bmatrix} \left(V_0 + V_1 + V_2 + V_3\right) \\ \left(V_4 + V_5 + V_6 + V_7\right) \\ \left(V_8 + V_9 + V_{10} + V_{11}\right) \\ -\left(V_6 - V_7 - V_8 + V_9\right) \\ -\left(V_{10} - V_{11} - V_0 + V_1\right) \\ -\left(V_2 - V_3 - V_4 + V_5\right) \end{bmatrix}^i - \frac{1}{4} \begin{bmatrix} i_{fx} \\ i_{fy} \\ i_{fz} \\ V_{fx} \\ V_{fy} \\ V_{fz} \end{bmatrix} \tag{12}$$

The reflected pulses are given by [12]

$$\begin{bmatrix} V_0 \\ V_1 \\ V_2 \\ V_3 \\ V_4 \\ V_5 \\ V_6 \\ V_7 \\ V_8 \\ V_9 \\ V_{10} \\ V_{11} \end{bmatrix}^r = \begin{bmatrix} V_x - i_y - V_1^i \\ V_x + i_y - V_0^i \\ V_x + i_z - V_3^i \\ V_x - i_z - V_2^i \\ V_y - i_z - V_5^i \\ V_y + i_z - V_4^i \\ V_y + i_x - V_7^i \\ V_y - i_x - V_6^i \\ V_z - i_x - V_9^i \\ V_z + i_x - V_8^i \\ V_z + i_y - V_{11}^i \\ V_z - i_y - V_{10}^i \end{bmatrix} \quad (13)$$

The incident voltages for the next time steps are found by swapping with the reflected voltages from the previous time step, i.e. the swap between ports 0 and 1 of the cells $\bar{z}$ and $\bar{z} - 1$ as the time step goes from k to k+1 is given by,

$$_{k+1}V_1^i\left(\bar{z}-1\right) = {}_kV_0^r\left(\bar{z}\right), \qquad {}_{k+1}V_0^i\left(\bar{z}\right) = {}_kV_1^r\left(\bar{z}-1\right) \quad (14)$$

At a boundary of the mesh a reflection coefficient is used to simulate different types of boundary such as a perfect electric conductor or a perfect magnetic conductor. TLM is a powerful tool for the modelling of electromagnetic problems. Later in this paper it is used to model, EMC problems containing thin wires, materials and electroabsorption modulators.

B. Finite Difference Time Domain Method

Like the TLM method described above the Finite Difference Time Domain method (FDTD) directly solves Maxwell's equations (see equation (1) in the previous section). The derivatives in the equations are replaced by finite differences. Unlike the TLM method in FDTD the electric and magnetic fields are not calculated at the same points in time and space. They are separated by half a time and space step.

For example in the one dimensional case, in free space, Maxwell's equations become.

$$\frac{\partial E_x}{\partial t} = -\frac{1}{\varepsilon_0}\frac{\partial H_y}{\partial z} \quad (15)$$

$$\frac{\partial H_y}{\partial t} = -\frac{1}{\mu_0}\frac{\partial E_x}{\partial z} \quad (16)$$

Using the central difference approximation for the spatial and temporal derivatives these equations become,

$$\frac{E_x^{n+1/2}(k) - E_x^{n-1/2}(k)}{\Delta t} = \frac{1}{\varepsilon_0}\frac{H_y^n\left(k+1/2\right) - H_y^n\left(k-1/2\right)}{\Delta x} \quad (17)$$

$$\frac{H_y^{n+1}\left(k+1/2\right) - H_y^n\left(k+1/2\right)}{\Delta t} = \frac{1}{\mu_0}\frac{E_x^{n+1/2}(k+1) - E_x^{n+1/2}(k)}{\Delta x} \quad (18)$$

From these equations it can be seen that the electric and magnetic fields have been separated in both time and space by half a step. The equations can be extended to the 3D case.

C. Finite Difference Beam Propagation Method

The Finite Difference Beam Propagation Method (FD-BPM) is one of the most widely used techniques in photonics. It is used to solve the Helmholtz equation shown below.

$$\nabla^2\varphi(x,y,z) + k_0^2 n^2 \varphi(x,y,z) = 0 \quad (19)$$

The basis of this method is to replace the partial derivatives in this equation with corresponding finite differences. Unlike the TLM and the FDTD methods described above this technique does not directly describe the electric and magnetic fields. Instead the fields are assumed to diverge slowly along a chosen axis of propagation. The field is therefore split into the envelope and a term that represents the propagation and only the envelope is modelled,

$$\varphi(x,y,z) = \phi(x,y,z)e^{-i\beta z} \quad (20)$$

where $\beta = k_0 n_0$, $k_0 = \omega / c$ with n_0 being a suitably chosen background refractive index.

This expression can be substituted back into equation (19). The partial differentials are then replaced by finite differences and can therefore be solved numerically. One difficulty for BPM is that a large matrix problem needs to be solved for each propagation step. This is particularly true in the 3-D case. Alternating direction implicit (ADI) schemes are typically used for 3D problems

In the section III (E) of this paper we look at the use of a wide-angle beam propagation method [13] to model tapered laser cavities. Techniques such as this are required because the traditional BPM is limited in the angular range of the principal propagation distance [14]. For simplicity, the wide angled schemes are described for the 2 dimensional case. The equation for the slowly varying envelope is then given by,

$$\frac{\partial^2\phi}{\partial z^2} - j2k_0 n_0 \frac{\partial\phi}{\partial z} + \frac{\partial^2\phi}{\partial x^2} + k_0^2\left(n(x,z)^2 - n_0^2\right)\phi = 0 \quad (21)$$

This equation can factorised,

$$\left(\frac{\partial}{\partial z} - j\beta + j\beta\sqrt{1+X}\right) \bullet \left(\frac{\partial}{\partial z} - j\beta - j\beta\sqrt{1+X}\right)\phi = 0 \quad (22)$$

where $\beta = k_0 n_0$. Considering only the forward waves this equation becomes,

$$\frac{\partial \phi}{\partial z} = -j\beta\left(\sqrt{1+X} - 1\right)\phi \quad (23)$$

where,

$$X = \frac{1}{\beta}\left[\frac{\partial}{\partial x^2} + k_0^2\left(n(x,z)^2 - n_0^2\right)\right] \quad (24)$$

Different approximations to the operator $\sqrt{1+X}$ lead to different BPMs. One of the most common is to use the higher order rational Padé equation [15]

$$\sqrt{1+X} - 1 = \frac{N_m(X)}{D_n(X)} \quad (25)$$

where $N_m(X)$ and $D_n(X)$ are polynomials of degree *m* and *n* respectively.

One method of computing equation (25) in an efficient manner that is valid for wide-angle propagation is to use a Padé series expansion. Full details can be found in [15]. The use of the FD-BPM method to describe the optical properties of a tapered waveguide laser will be described in section III(E).

D. Semi-analytical Methods

In some cases the problem can be further simplified if the system being investigated meets certain criteria. For example the Spectral Index (SI) method [6] and Half Space Radiation Mode (HSRM) [16] can be used where a low refractive index (i.e. air) is used in a structure. The Free Space Radiation Mode (FSRM) [3] method can be used when the variation in the transverse refractive index is less than 10%.

In the SI method the semiconductor-air boundary is replaced by a polarisation dependent evanescent boundary at which the field set to zero. Exact solutions are then found for the field in both the rib region and the substrate region. These solutions are matched along the boundary using a variational principle, i.e. minimising the difference in the derivatives of the field across the boundary. This gives a simple transcendental Eigenvalue equation for the longitudinal propagation constant β. [17]

III. APPLICATIONS

In this section we examine some current applications of the numerical techniques listed above as well as some of the more recent developments that have improved the range of applications. Firstly, the use of TLM to describe fine features such as thin wires will be examined. There follows sections on triangular meshes, materials and electroabsorption modulators. This latter problem involves the description of both microwave and optical signals. Finally there will be an application of FD-BPM to model the optical properties of tapered laser cavities.

A. Description of fine wires

Modelling of electromagnetic problems where all features are of the same scale is relatively simple. A standard, regular Cartesian grid can be used to discritise the problem and the calculations can be carried out using a numerical technique such as TLM of FDTD as described above. Difficulties arise when different length scales are involved in the problem, such as a large equipment cabinet that contains fine wires. It is impractical to reduce the size of the mesh throughout the cabinet to the length scale of the wire due to the computational time and memory required.

One method used to describe small features is to distort the mesh locally. Various methods of doing this have been investigated for both FDTD and TLM. The two main ways are given in Fig 2. This shows a standard mesh, a multi-grid mesh, which is a localised refinement of the mesh and a hybrid mesh. In the hybrid mesh the grid refinement is still localised, but stretches to the edges of the grid.

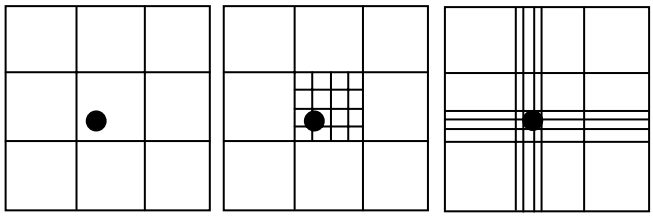

(a) (b) (c)

Fig 2. Various types of mesh for TLM calculations (a) regular mesh, (b) multigrid mesh, (c) hybrid mesh

In these schemes computational efficiency is maintained because the mesh is only refined locally. This is particularly true in 2 (b). However there are problems with this method as at the interface between the coarse and fine grids the information is available at a different temporal and spatial granularity from the two grids. This means that the information from the fine grid has to be averaged to allow it to be transferred to the coarse grid.

There have been many methods used to interface between the coarse and fine grids in both FDTD [18,19,20,21,22,23] and TLM [24,25,26,27] calculations. The methods used in the above references all aim to reduce reflections and increase stability at the boundary. As an equivalent circuit field representation TLM should have guaranteed stability as long as the interface can be represented as a passive lossless circuit. This means that charge and energy are conserved and no reflections or delays are present. In practice stable methods can be devised with some energy loss at high frequencies. A comparison between the FDTD and TLM methods in ref [28] suggests that the TLM method is the more robust. The use of

triangular meshes as an interface will be discussed in section B.

A more elegant solution, than simply reducing the mesh size locally is to find a local solution for the field around a thin wire and map it onto the mesh. This can be done in several ways in FDTD [29, 30, 31] and TLM [32, 33].

Recent developments have included obtaining an exact analytical description of the electromagnetic fields that can then be modelled numerically [34, 35]. This allows accurate modelling of an arbitrarily placed thin wire in a coarse mesh.

In this method the electromagnetic field around the wire is described in cylindrical co-ordinates using Bessel $J(k_0 r)$ and Neumann functions $N(k_0 r)$.

$$E_z(r,\varphi) = \sum_{n=-\infty}^{\infty} B_n e^{jn\varphi}\left[J_n(k_0 r) + D_n N_n(k_0 r)\right] \quad (26)$$

where B_n and D_n are constants and

$$k_0 = \omega\sqrt{\varepsilon_0 \mu_0} \quad (27)$$

The boundary condition that the tangential field E_z is zero on the surface of the wire (radius $r = a$) gives that

$$D_n = -\frac{J_n(k_0 a)}{N_n(k_0 a)} \quad (28)$$

substituting into (26) gives

$$E_z(r,\varphi) = \sum_{n=-\infty}^{\infty} B_n e^{jn\varphi}\left[J_n(k_0 r) - \frac{J_n(k_0 a)}{N_n(k_0 a)} N_n(k_0 r)\right] \quad (29)$$

$$H_\varphi(r,\varphi) = \frac{1}{j\omega\mu_0}\frac{\partial E_z}{\partial r} \quad (30)$$

This then represents the fields around the wire, exactly, as a superposition of cylindrical wave modal solutions. These exact solutions are then mapped onto the coarse mesh taking into account the position of the wire. This mapping requires the use of known summation theorems for Bessel functions [36], i.e. if $Z_m(x) = aJ_m(x) + bN_m(x)$ with a and b independent of m and x.

$$e^{j\omega\varphi} Z_v(kR) = \sum_{m=-\infty}^{\infty} e^{jm\phi} J_m(kr) Z_{v+m}(kr_0) \quad (31)$$

where $R = \sqrt{r^2 + r_0^2 - 2rr_0\cos(\phi)}$, r, r_0 are sides of a triangle with ϕ the angle between r and r_0, φ is the angle between r_0 and R. Fig 3 shows an offset wire on a two dimensional TLM node, the field expansions around the wire can be mapped evaluated at the required positions (V_0, V_1, V_2, V_3) on the TLM node.

Numerical results for this technique show good agreement with analytical results for both centred and offset wires. Excellent accuracy of this method was found for a broad range of frequencies and the method can predict the small phase changes in the reflected field when a wire is offset. A similar technique has been formulated to describe thin wires in 3D [37]

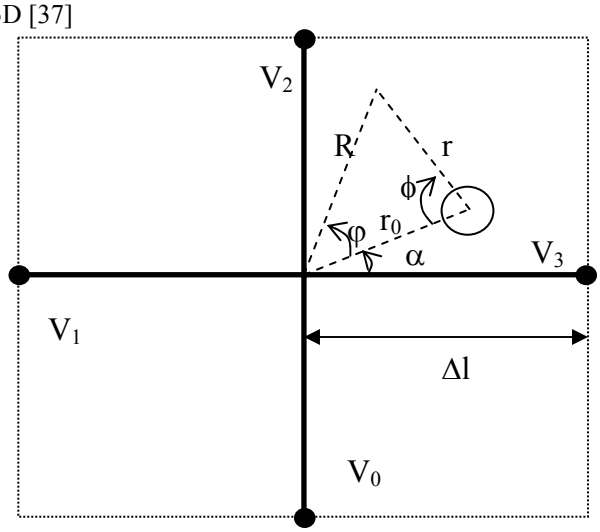

Fig. 3. Offset wire on a 2D TLM node

B. Triangular meshes

A recent development that has provided a new way to interface between coarse and fine meshes is the use of triangular meshes. Standard meshes used in two dimensional TLM and FDTD are based on rectangles with 4 ports to each node, i.e. the node consists of two transmission lines meeting at a right angle. In triangular meshes three transmission lines are present giving three ports [10, 11]. This gives greater flexibility to conform to curved boundaries and can be exploited to interface between regions of the mesh with different spatial and temporal resolution

The parameters of a triangular node (shown in Fig 4) are not entirely arbitrary and must meet the Delaunay criterion [38]. This is common to many unstructured mesh techniques and is not difficult to enforce. Meshes of this type are available from standard meshing software.

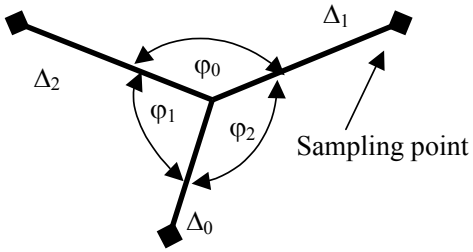

Fig. 4. Schematic of a triangular TLM node

The equivalent circuit parameters of the transmission line network shown above and the electric and magnetic fields are found by expanding the field around the node centre in cylindrical harmonics. This is similar to the method described above for the thin wire calculations. From the expansion the field modal impedances E/H can be calculated and a network that produces the same modal impedances, V/I, can be constructed. The equivalences calculated in this way are valid

up to a maximum frequency of $f_{\max}$ corresponding to a spatial resolution of $\lambda_{\min}/10$. The transmission lines in Fig 4 have total inductances and capacitances given by;

$$L_i = \frac{\mu_0 \Delta_i}{l_i}, \qquad C_i = \frac{\varepsilon_0 \Delta_i l_i}{2}, \qquad i = 0,1,2 \qquad (32)$$

where l_i is the length of the triangle side that Δ_i passes through. Link and stub lines can be combined to model the required inductance and capacitance.

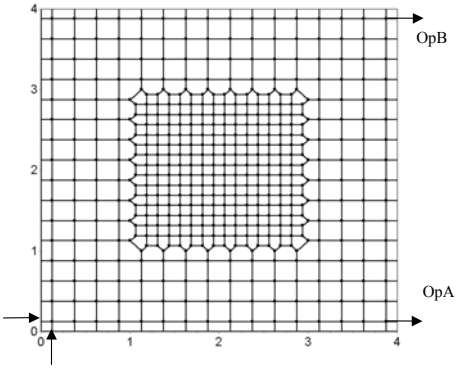

Fig 5. Multi-grid Rectangular TLM stitched together with triangular TLM nodes

In order to test the triangular meshes the example given in Fig 5 was modelled in reference [10]. This problem has a coarse mesh surrounding an area with a fine mesh (ratio 2:1). The interface between the two meshes is created using triangular nodes. A pulse is injected at the point (0,0) and the output field at both OpA and OpB is examined. For comparison, the case where just a coarse mesh is used was also calculated.

Fig 6 shows the relative error against normalised frequency at both OpA and OpB. The relative error is always less than 1%. It is possible to use the same technique where there is a greater difference between the coarse and fine meshes.

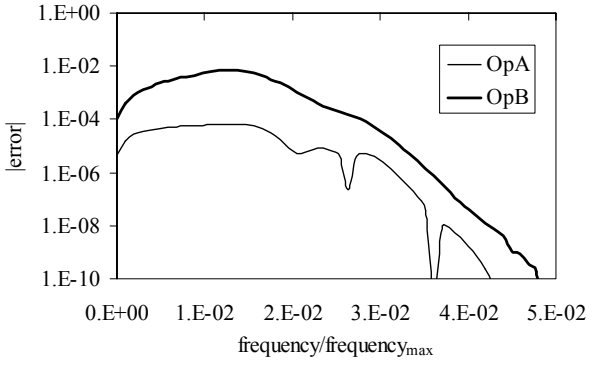

Fig 6. Results for the example shown in Fig 5 showing relative error in frequency domain at OpA and OpB

The use of triangular meshes can provide a stable and efficient interface between coarse and fine meshes which is of great importance in multiscale problems. Triangular meshes can also be used to give a variable mesh size across an entire structure and can be used to give more accurate meshing of shapes that do not fit well with Cartesian meshes such as curved surfaces.

C. Materials

Time domain techniques such as FDTD and TLM are particularly well suited to the modelling of the interaction between materials and electromagnetic waves. By using a pulse excitation the response of a material over a wide bandwidth can be obtained in a single simulation. For frequency domain simulations many calculations would be required to obtain the same information. In order for the solution to be valid over the wide bandwidth the frequency response of the material must be included in the algorithm. Time domain techniques are also better able to handle nonlinear materials as they can properly describe the frequency mixing effects that result in the generation of harmonics.

The advantage of TLM over FDTD in the description of materials is that in FDTD the time electric and magnetic fields are offset by half a step in both time and space. As a result of this, coupling between the fields can only be carried out using averaging techniques, however, much work has been done on the description of materials using FDTD. In TLM the electric and magnetic fields are available in the same time and space.

The use of *Z*-transform methods to discritise the constitutive relations was first introduced for TLM in [39] after first being used with FDTD. It has since been extended to anisotropic [40], chiral [41] and nonlinear [42, 43] materials. The *Z*-transform is particularly useful because in the *Z*-domain convolutions become simple multiplications. In this paper the technique is reviewed and its use is demonstrated.

In the modelling of materials with TLM the material properties are included in the connection process when the incident and reflected voltages are swapped between nodes. In the method developed in [39] and extended in [40, 41, 42] the material properties are contained in a matrix *t*. For the case of an isotropic material, the following matrix applies,

$$\begin{bmatrix} V_x \\ V_y \\ V_z \\ i_x \\ i_y \\ i_z \end{bmatrix} = \begin{bmatrix} t_{ex} & & & & & \\ & t_{ey} & & & & \\ & & t_{ez} & & & \\ & & & t_{mx} & & \\ & & & & t_{my} & \\ & & & & & t_{mz} \end{bmatrix} \begin{bmatrix} V_x \\ V_y \\ V_z \\ -i_x \\ -i_y \\ -i_z \end{bmatrix}^r$$

For anisotropic materials and nonlinear materials more elements of the matrix *t* are required. The matrix *t* contains terms relating to the electric conductivity, susceptibility and coupling terms for the electric elements and the magnetic resistivity and susceptibility along with coupling terms for the magnetic elements.

Two examples of the use of this method to model the electromagnetic properties of materials are given in this paper. Firstly an Air-Lorentz material interface is shown. Fig 7 shows the field after 737.5ps. The interface is marked on the graph by the vertical line at 0.0125m, the initial pulse, on the left hand side has been scaled down by a factor of 10. Full details are contained in [39].

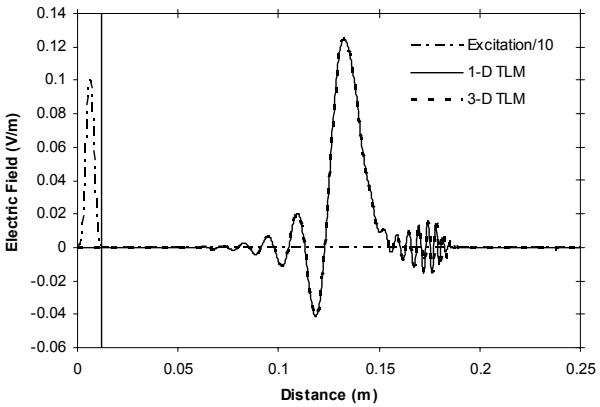

Fig.7. Air-Lorentz interface showing the field after 737.5ps

Fig. 8 is an illustration of the Faraday rotation where, by using four different slab depths illuminated with a sinusoidal source of frequency 182GHz, the rotation of a linearly polarized wave as it passes through the slab is observed. Full details are contained in [40].

TLM provides a stable and accurate method of modelling the interaction of electromagnetic wave with materials. As it is a time domain method results from a single simulation are valid over a wide bandwidth and unlike FDTD the electric and magnetic fields are available at the same time and space leading to a simpler implementation. Further application of the *Z*-transform technique to the simulation of optical switches and fibre Bragg gratings, including the effects of material dispersion can be found in [44]

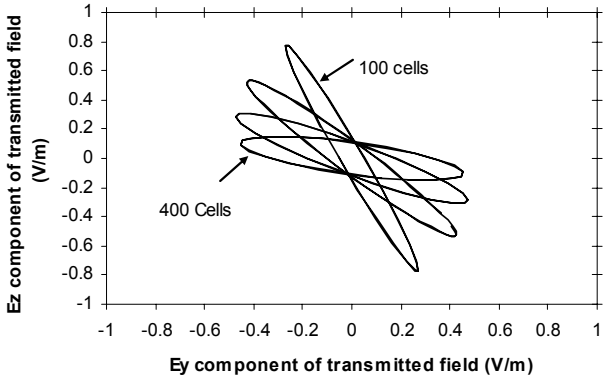

Fig. 8. Faraday rotation in magnetised plasma,

D. Modelling of the Microwave Properties of Electroabsorption Modulators

The RF modulator is a key device in dense wavelength division multiplexing (DWDM) and optically time division multiplexing systems (OTDM) as it directly determines both the operating frequency and the bandwidth of a system. The principal function of the modulator is to imprint the microwave signal onto the optical carrier. Accurate modelling and optimisation of these devices is seen as a way forward in increasing the systems' bandwidth and hence improving devices' performance. However, their modelling remains challenging due to the need to simultaneously model two different parts of the modulator, namely microwave and optical.

In this paper we concentrate on modelling of microwave properties of two different types of electroabsorption (EA) modulators namely, lumped EA modulators (L-EAM) based on a microstrip line and travelling wave EA modulators (TW-EAM) based on a coplanar transmission line**.** In lumped EA modulators an applied electric field causes the multiple quantum wells (MQWs), embedded in the optical waveguide, to change the insertion loss of the optical guide, typically in the range of around 15-20 dB/mm and bandwidths as high as 50 GHz have been reported [45]. The distinctive feature of TW modulators is that the modulating electrical signal propagates in the same direction and ideally at the same speed as the optical signal, causing the phase modulation induced by the electrical signal to accumulate along the propagation length. TW modulators can further extend the bandwidth of the modulator (up to 100 GHz) and are now preferred choice for many broadband applications.

The time domain Transmission-Line Modelling method [1] (TLM) is ideally suited for accurate modelling of microwave characteristics of EA modulators, taking into account their complex geometries and material parameters. The TLM method will be used to model the microwave characteristic impedance and effective dielectric constant (ε_{eff}) of lumped and TW EA modulators, and investigate the effect the finite metal thickness has on these two microwave parameters.

The TLM method with the graded mesh [8] is used. This allows finer mesh to be applied for modelling of small features, namely thin metal layers, the MQW region and additional thin layers, while at the same time a coarser mesh is used for modelling larger features such as air and the substrate region.

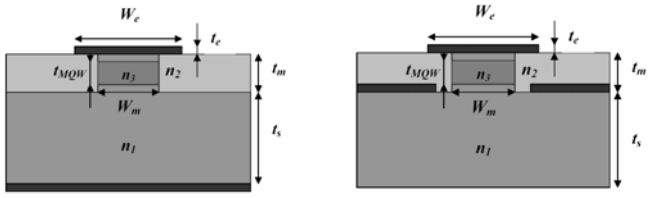

(a) (b)

Fig. 9. L-EAM (a) and TW-EAM (b) cross-section geometries.

i. Numerical results

The schematic presentation of the cross-sectional geometries of a microwave line of the lumped EA modulator and a coplanar waveguide of the TW EA modulator modelled in this section are shown in Fig 9. EAMs of similar geometries were fabricated and presented in [46, 47].

In the Fig 9 parameters n_1, n_2, and n_3 represent refractive indices of InP, As doped silica and InGaAsP respectively; t_e, t_m, t_{MQW}, t_s represent thickness of electrodes, mesa, multiple quantum well, and substrate, respectively, and W_e and W_m are widths of the p-electrode and the mesa. The p- and n-electrodes in Fig 9(b) overlap by 0.6 μm. The TLM method is used to investigate the influence of p-electrode width and finite electrode thickness on the microwave characteristics of the EAMs.

Initialisation of both structures is done with a Gaussian pulse of duration of 10^{-14} s. The time dependent currents and voltages are then extracted and fast Fourier transformed to give the frequency dependent currents and voltages. These are then used to calculate the characteristic impedance Z_c, effective dielectric constant ε_{eff} and propagation constant β as

$$Z(f)=\frac{V(f)}{I(f)}, \varepsilon_{eff}(f)=\frac{\beta c}{2\pi f}, \beta=-\frac{\ln\left(\frac{V_1(f)}{V_2(f)}\frac{|V_2(f)|}{|V_1(f)|}\right)}{i\Delta z},$$

where V and I are voltages and currents of the line, c is the speed of light, f is the frequency, V_1 and V_2 are voltage spectrums at the distance of Δz.

The frequency dependence of the impedance and the effective refractive index versus electrode width W_e for lumped and TW EA modulator are shown in Fig 10 (a, b). The parameters for the lumped modulator, Fig 9(a), are: n_1=3.53, n_2=1.63, n_3=3.68, t_e=0 or 0.33 μm, t_m=2 μm, t_{MQW}=0.33 μm, t_s=6 μm. The results are shown for electrode width W_e=8 μm (solid lines) and 6 μm (dashed lines). It can be seen that the impedance decreases with increasing of electrode width whilst the effective dielectric constant decreases. This behaviour is similar to classical microstrip lines [48]. Moreover, values for the impedance change about 1% over the region of 150 GHz, which is typical of ordinary microstrip lines with InP substrate thicknesses of the order of 10 μm.

Similar behaviour is noticed for the TW EAM geometry where the corresponding electrode widths were 10 μm (solid lines) and 6 μm (dashed lines), Fig 10(b), whilst all other parameters remain the same as for the Fig 10(a). The lumped EA geometry considered has impedance close to or higher than 50 Ω whilst the TW-EA geometry considered has impedances lower than 50 Ω. Thus in both cases specific geometries of the modulators pose a problem when matching to a 50Ω feed line is required. This effect is more pronounced for the TW-EAM geometry.

As the optical field propagates in the MQW layer, in the case of the TW modulator it is required that the velocities of the optical and microwave fields are matched which implies that the effective dielectric constants of the microwave and optical fields are equal. However, the stronger frequency dependence of the effective dielectric constant of the TW EAM for the microwave field adds to the difficulty of matching to the effective refractive index of the optical field and furthermore introduces undesirable dispersion effects.

Fig 11 shows the effect of the finite electrode thickness on the spectral characteristics of impedance and effective dielectric constant of EA modulators. The lumped EAM structure analysed is the same as for Fig.10 with W_e=6 μm and electrode thicknesses of 0 μm (solid lines) and 0.33 μm (dashed lines), Fig 11(a). It can be seen that increasing the electrode thickness increases both the impedance and the effective refractive index. Moreover, the finite metal thickness causes a much stronger frequency dependence of the effective refractive index. In the case of the TW EAM the results are shown in Fig 11(b) for the case of the electrode width W_e=6 μm and electrode thickness of 0 μm (solid lines) and 0.33 μm (dashed lines). It can be seen that finite metal thickness decreases both the impedance and the effective dielectric constant of the TW EAM. In both cases, the influence of the finite electrode thickness cannot be neglected and must be taken into account for accurate modelling of EAMs.

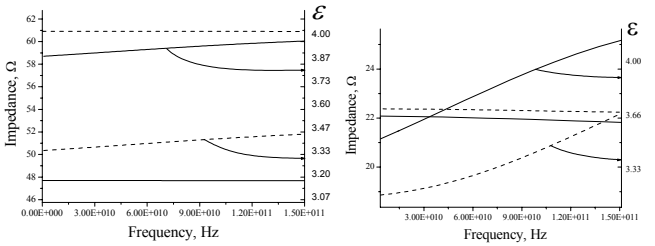

(a) (b)

Fig. 10. Impedance and effective dielectric constant for (a) lumped-EAM, W_e=8 μm (solid line and W_e=6 μm dashed lines) and (b) TW-EAM geometry; (W_e=10 μm (solid lines) and W_e=6 μm (dashed lines).

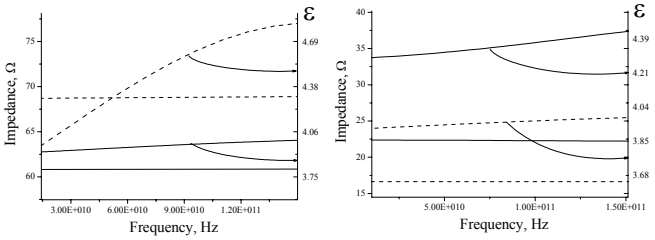

(a) (b)

Fig. 11. Impedance and effective dielectric constant for (a) lumped-EAM, W_e=6 μm, and (b) TW-EAM geometry W_e=6 μm. In both cases t_e=0 μm (solid lines) and t_e=0.3 μm (dashed lines).

E. Tapered Laser Cavities

Tapered laser cavities [49] are another example of a multi-physics problem in photonics. Not only are the optical properties important, but the electrical and thermal properties also significantly affect performance.

A tapered waveguide laser consists of a straight waveguide section and a tapered amplifier section as shown in Fig 12. The straight section acts as a modal filter to ensure that the amplifier is only excited by the fundamental mode. The tapered section gradually lowers the optical power density by allowing the beam to expand. This minimizes effects such as spatial hole burning and catastrophic mirror damage while permitting an increase in the total output power.

Due to the structure of the laser cavity a wide angled BPM method must be used as described previously. For the laser cavity the permittivity (ε) depends on the temperature and the carrier distributions that in turn depend on the optical field intensity and the injection current. The carrier concentrations are found by solving the Poisson equation for both electrons and holes. Full details can be found in [50]. In the discussion of the WA-BPM technique the permittivity was contained in the refractive index since $n=\sqrt{\varepsilon\mu_0}$

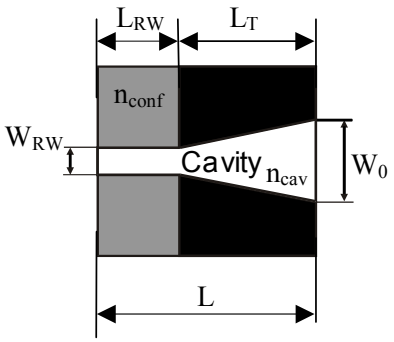

Fig. 12. Two dimensional representation of a tapered laser cavity

The calculation is carried out using the coupled solution method. This method sub-divides the cavity into slices. The electronic and thermal equations are solved for a slice of the cavity. This gives new values for the refractive index and gain profiles of the slice, these values are then used as the optical field propagates to the next slice.

The results of this model have been compared with experiment in [50]. A laser cavity with L=2mm, W_{RW}=0.75mm, W_0=90.3µm, R_{RW}=95%, R_0=1% and Δn_{eff}=0.008 is used. The virtual source power distributions for a variety of output powers show good agreement as shown in Fig 13.

The use of modelling of components such as tapered laser cavities can provide information on the interaction between the various parameters that affect performance, such as the effect of the electric and thermal properties on optical performance. This can improve the efficiency of component design and therefore reduce the cost of the design process.

IV. CONCLUSIONS

Numerical modelling is an important tool in electromagnetics. The development of faster computers can improve the performance of numerical models, however greater improvements and understanding can be gained from the development of new numerical techniques.

In this paper some recent developments in TLM and FD-BPM modelling have been discussed and examples of their use given. Amongst these, the description of fine details in larger problems is of particular interest for EMC calculations. Two recent developments, the use of exact solutions for the field round a fine wire mapped onto the numerical grid and the use of triangular meshes to interface between coarse and fine meshes were presented. The use of TLM to describe the interaction of EM fields and materials was also described with the examples of an air-Lorentz interface and Faraday rotation in magnetized plasma.

In photonics numerical modelling can also be used to improve the design of components. In this area the design of an EA modulator and a tapered laser cavity were given as examples.

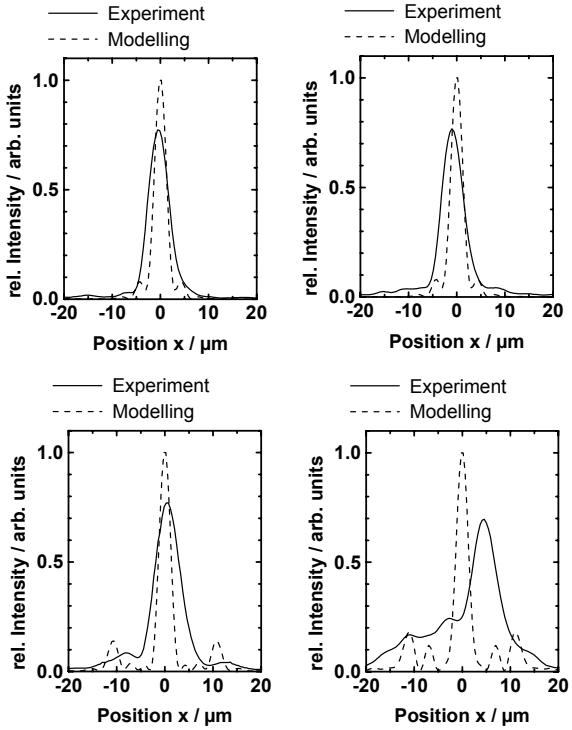

Fig. 13. Virtual source power distributions (a) P=0.5W, (b) P=1W, (c) P=1.5W and (2) P=2W.

REFERENCES

[1] C. Christopoulos, *The Transmission-Line Modeling Method-TLM*. New York. IEEE Press, 1995

[2] A Taflove, *Computational electrodynamics, The Finite Difference Time-Domain Method*. Norwood MA. Artech House 1995.

[3] J.L. Volakis, A. Chaterjee, L.C. Kempel, *Finite Element Method for Electromagnetics*. New York, IEEE Press, 1998

[4] R.F. Harrington, *Field Computation by Moment Methods* New York, McMillan, 1968

[5] J. Yamauchi. *Propagating Beam Analysis of Optical Waveguides*. Research Studies Press Ltd 2003

[6] P. N. Robson, P. C. Kendall (Eds), *Rib waveguide theory by the Spectral Index Method*, Research Studies Press 1990

[7] C. J. Smartt, T. M. Benson, P. C. Kendall 'Free Space Radiation Mode' method for the analysis of the propagation in optical waveguide devices, *IEE Proceedings-J Optoelectronics.* Vol. 140 No. 1, pp. 56-61, 1993

[8] SV Boriskina, P Sewell, TM Benson, AI Nosich, Accurate simulation of 2D optical microcavities with uniquely solvable boundary integral equations and trigonometric-galerkin discretisation *JOSA A* Vol. 21, pp. 393-402, 2004

[9] F.V. Fedotov, A.G. Nerukh, T.M. Benson, P. Sewell Investigation of electromagnetic field in a layer with time-varying medium by Volterra integral equation method, *Journal of Lightwave Technology* Vol. 21 pp. 305-314, 2003

[10] P. Sewell, J. Wykes, A. Vukovic, D. W. P. Thomas, T. M. Benson C. Christopoulos, Multi-grid interface in Computational electromagnetics, *Elec. Lett*. Vol. 40 No. 3, pp 162-163, 2004

[11] P. Sewell, J. Wykes, T. M. Benson, C. Christopoulos, D. W. P. Thomas, A. Vukovic, Transmission-Line modelling using unstructured Triangular meshes, *IEEE Trans MTT*, Vol. 52, No. 5, pp. 1490-1497, 2004

[12] V Trenkic, C Christopoulos, T. M. Benson, Simple and elegant formulation of scattering TLM nodes, *Elect. Lett*, Vol. 29, No. 18 pp 1651-1652, 1993

[13] T Anada, T Hokazono, T Hiraoka J P Hsu, T M Benson, P Sewell, Very-wide-angle beam propagation methods for integrated optical circuits, *IEICE Trans Electron*, Vol E82-C, No. 7, pp 1154-1158 1999

[14] N P Holting, R Marz, Results of benchmark tests for different numerical BPM algorithm, *J. Lightwave Technol*. Vol. 13, pp 216-224, 1995

[15] G R Hadley, Wide-Angle beam propagation using Padé approximant operators, *Opt Lett*, Vol 17, No. 20, pp 1426-1428, 1992

[16] A Vukovic, P Sewell, T M Benson, P C Kendall, Novel half space radiation mode method for buried waveguide analysis *Optical and Quantum Electronics,* Vol. 31 pp. 43-51, 1999

[17] S. Greedy, P. Sewell, A. Vukovic, T.M. Benson, Efficient analysis of integrated optical circuits by the spectral index method, *Microwave and Optical Technology Letters,* Vol. 38, pp. 68-73, 2003

[18] K.S. Kunz, L. Simpson, A Technique for increasing resolution of finite-difference solution to Maxwell's equations. *IEEE Trans on EMC,* Vol 23, pp 419-422, 1981

[19] I.S. Kim, W J R Hoefer, A local mesh refinement algorithm for the FDTD method using Maxwell's curl equations, *IEEE Trans. On MTT,* Vol. 38, pp 812-815, 1990

[20] D. T. Prescott, N. V. Shuley, A method for incorporating different sized cells into the finite-difference time-domain analysis technique, *IEEE Microwave and Guided Wave Letters*, Vol 2. pp 434-436, 1992

[21] K. M. Krishnaiah, C.J. Railton Passive, Equivalent circuit of FDTD, An Application to subgridding, *Elec Lett*, Vol 33, pp 1277-1278, 1997

[22] K. M. Krishnaiah, C.J. Railton, A Stable subgridding algorithm and its application to Eigenvalue problems, *IEEE Trans on MTT*, Vol 47, pp 620-628. 1999

[23] M. J. White, Z Yun, M. F. Iskander, A new 3D FDTD multigrid technique with dielectric traverse capabilities, *IEEE Trans on MTT,* Vol. 49 pp 422-430, 2001

[24] J. L. Herring, C. Christopoulos, Multigrid TLM method for solving EM field problems, *Elec Lett*, vol. 27, pp 1794-1795, 1991

[25] J. L. Herring, C. Christopoulos, Solving EM field problems using a multiple grid TLM method. *IEEE trans on Antennas and Propagation*, Vol 42, pp 1654-1658, 1994

[26] J. L. Herring, C. Christopoulos, The application of different meshing techniques to EMC problems, *Proc Annual Rev of progress in Applied Computational Electromagnetics*, Monterey, pp 755-762, 1993

[27] J. Wlodarczyk, A new multigrid interface for the TLM method, *Elec Lett*, Vol 32, pp 1111-1112, 1996

[28] F. J. German, J. A. Svigeli, R. Mitra, A numerical comparison of dispersion in irregular graded TLM and FDTD meshes, 12th *Annual Review of Progress in Applied Computational Electromagnetics*, Monterey, 270-278, 1996

[29] R Holland, J.W. Simpson, Finite-difference analysis of EMP coupling to thin struts and wires. *IEEE Trans. On Electromagnetic Compatibility* Vol. 23 pp 88-97, 1981

[30] G Ledfelt, A stable subcell model for arbitrarily oriented thin wires for the FDTD method. *International Journal of Numerical Modelling-Electronic Networks Devices & Fields*. Vol. 15 pp 503-15, 2002

[31] F Edelvik, A new technique for accurate and stable modelling of arbitrarily oriented thin wires in the FDTD method. *Uppsala University Report 2002-016* (www.it.uu.se/research/reports/2002-016/)

[32] J Wlodarczyk, D P Johns, New wire interface for graded 3D TLM. *Elec Lett*, Vol. 28, pp 728-729 1992

[33] J A Porti, J A Morente, M Khallidi, A Gallego, Comparison of thin wire models for the TLM method, *Elec Lett*, vol. 28, pp 1910-1911, 1992

[34] Y K Choong, P Sewell, C Christopoulos, New thin wire formulation for time-domain differential equation models, *Int. J. Numer. Model*, Vol 15, pp 489-501, 2002.

[35] Y K Choong, P Sewell, C Christopoulos, Accurate modelling of an arbitrary placed thin wire in a coarse mesh, *IEE Proc-Sci. Meas. Technol*. Vol 149, no. 5, pp 250-253, 2002

[36] P M Morse, H Feshbach, *Methods of Theoretical Physics*, Second Edition, McGraw-Hill, New York, 1953

[37] P Sewell, Y K Choong, C Christopoulos, An Accurate thin-wire model for 3D TLM simulations, *IEEE Transactions on Electromagnetic compatibility*, Vol 45 pp 207-217, 2003

[38] J R Shewchuk, Lecture notes on Delaunay mesh generation, http://citeseer.nj.nec.com/shewchuk99lecture.html 1999

[39] J Paul, C Christopoulos, D W P Thomas, Generalized Material Models in TLM-Part 1: Materials with Frequency-Dependent Properties, *IEEE Trans on Antennas and Propagation*, Vol 47, No. 10, pp 1528-1534, 1999

[40] J Paul, C Christopoulos, D W P Thomas, Generalized Material Models in TLM-Part 2: Materials with Anisotropic Properties, *IEEE Trans on Antennas and Propagation*, Vol 47, No. 10, pp 1535-1542, 1999

[41] J. Paul, C Christopoulos, D. W. P. Thomas Time-Domain Modelling of Electromagnetic Wave Propagation in Complex Materials *TLM Special Issue of Journal of Electromagnetics* Vol. 19, pp. 527-546, 1999

[42] J Paul, C Christopoulos, D W P Thomas, Generalized Material Models in TLM-Part 3: Materials with Nonlinear Properties, *IEEE Trans on Antennas and Propagation*, Vol 50, No. 7, pp 997-1004, 2002

[43] V Janyani, A Vukovic, J Paul, P Sewell, T M Benson, The Development of TLM models for nonlinear optics, *Microwave Review,* Vol. 10, pp 35-42, 2004

[44] Janyani V, Paul J, Vukovic A, Benson T.M., Sewell P TLM Modelling of Nonlinear Optical Effects in Fibre Bragg Gratings *IEE Proceedings Optoelectronics*. 151(4). pp 185-192, 2004,

[45] G. L. Li, P .K. L. Yu, "Optical Intensity Modulators for Digital and Analogue Applications", *J. of Lightwave Technology*, Vol.21, No.9, pp. 2010-2030, 2003.

[46] D. G. Moodie, P. J. Cannard, A. J. Dann, D. D. Marcenac, C. W. Ford, J. Reed, R. T. Moore, J. K. Lucek and A. D. Ellis "Low polarisation sensitivity electroabsorption modulators for 160 Gbit/s networks", *Elec. Lett.*, Vol.33, No.24, pp. 2068-2070, 1997.[47] S. Irmscher, R. Lewén, and U. Eriksson, "InP-InGaAsP high-speed travelling-wave electroabsorption modulators with integrated termination resistors," *IEEE Photon. Technol. Lett.*, vol. 14, pp. 923–925, July 2002.

[48] Robert E. Collin, *Foundation for microwave engineering*, McGraw-HILL International Editions, 1992.

[49] S Sujecki, J Wykes, P Sewell, A Vukovic, T M Benson, E C Larkins, L Borruel and I Esquivias. Optical properties of tapered laser cavities, *IEE Proc. Optoelectron*. Vol 150, No 3, pp 246-252, 2003

[50] S Sujecki, L Borruel, J Wykes, P Moreno, B Sumpf, P Sewell, H Wenzel, T M Benson, G Erbert, I Esquivias, E C Larkins, Nonlinear properties of tapered laser cavities. *IEEE Journal of selected topics in quantum electronics*, Vol 9, No. 3, pp 823-834, 2003